ACS NANO

www.acsnano.org

ARTICLE

Room-Temperature CrI_3 Magnets through Lithiation

Zhongxuan Wang, Huafei Zheng, Amy Chen, Lei Ma, Stephanie J. Hong, Efrain E. Rodriguez, Taylor J. Woehl, Su-Fei Shi, Thomas Parker, and Shenqiang Ren*

Cite This: *ACS Nano* 2024, 18, 23058–23066

Read Online

ACCESS | Metrics & More | Article Recommendations | Supporting Information

ABSTRACT: **The pursuit of two-dimensional (2D) magnetism is promising for energy-efficient electronic devices, including magnetoelectric random access memory and radio frequency/microwave magnonics, and it is gaining fundamental insights into quantum sensing technology. The key challenge resides in overseeing magnetic exchange interactions through a precise chemical reduction process, wherein manipulation of the arrangement of atoms and electrons is essential for achieving room-temperature 2D magnetism tailoring in a manner compatible with device architectures. Here, we report an electrochemically crafted CrI_3 layered magnet—a van der Waals material—with precisely tailored lithiation and delithiation degrees. The crystalline and packing structure within the intralayer are preserved during the lithium intercalation within the interlayer, owing to weak interlayer coupling. Intrinsic ferromagnetism featuring a Curie temperature reaching 420 K has been unequivocally demonstrated, showcasing a coercivity of 1120 Oe at room temperature. The degree of lithiation through the reduction from Cr^{3+} to Cr^{2+} plays a crucial role in determining a 28.5% change in magnetization and a 0.29 eV shift in the bandgap. Room temperature ferromagnetism and magnetoelectricity are critical for noncontact, specifically photon-driven, dynamic magnetism control of 2D magnet-based magnonics devices.**

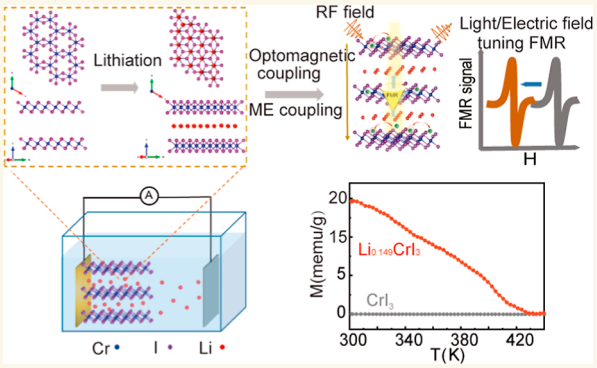

KEYWORDS: *lithiation, in-situ electrochemical lithiation, room temperature 2D magnetism, intercalation, light-induced modulation*

Magnets that display modulated ferromagnetic (FM) resonance and spin waves, either through magnetic field manipulation or spin-current injection, have attracted considerable attention in the realm of energy-efficient microwave (MW) electronics.[1,2] Its tailored magnetic response at high frequencies endows them with distinct advantages in radio frequency communication and detection.[3−5] However, the majority of MW devices are often reliant on bulk materials—ferrites, metals, and alloys—making the integration of nanoscale devices challenging attributed to their bulky size, high density, and the parasitic loss at high frequencies.[6−9] Conversely, two-dimensional (2D) magnets exhibit distinct advantages such as low dimensionality, large magnetic anisotropy, lightweightness, and stimuli responsiveness.[10−14] The pursuit of 2D layered magnets with magnetism control offers opportunities for exploring innovative designs to manipulate their room temperature magnetic properties. Due to finely modulated magnetism in low dimensions, 2D magnets hold immense promise for emerging energy-efficient devices.[15−17] Despite the intrinsic FM order in discovered 2D van der Waals (vdW) materials, it has often been characterized by a low Curie temperature (T_C). Moreover, many reported 2D magnetic materials rely on techniques like electrolyte gating, voltage tailoring, or high pressure for magnetism control, limiting their applications in nondisruptive magnonics. Elevating the Curie temperatures of 2D magnets, especially those surpassing room temperature, continues to be a central focus of ongoing research. Furthermore, there is an urgent need to achieve noncontact magnetism control in layered magnets with intrinsic ferromagnetism, including strong perpendicular anisotropy and, crucially, compatibility with photon-driven control.

The electrochemical method stands out as a highly effective strategy for the tunable and controllable manipulation of 2D magnetic materials through the introduction of in situ and real-time reduction processes.[18,19] This method involves leveraging

Received: April 20, 2024
Revised: August 8, 2024
Accepted: August 9, 2024
Published: August 14, 2024

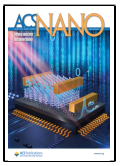

https://doi.org/10.1021/acsnano.4c02613
ACS Nano 2024, 18, 23058−23066

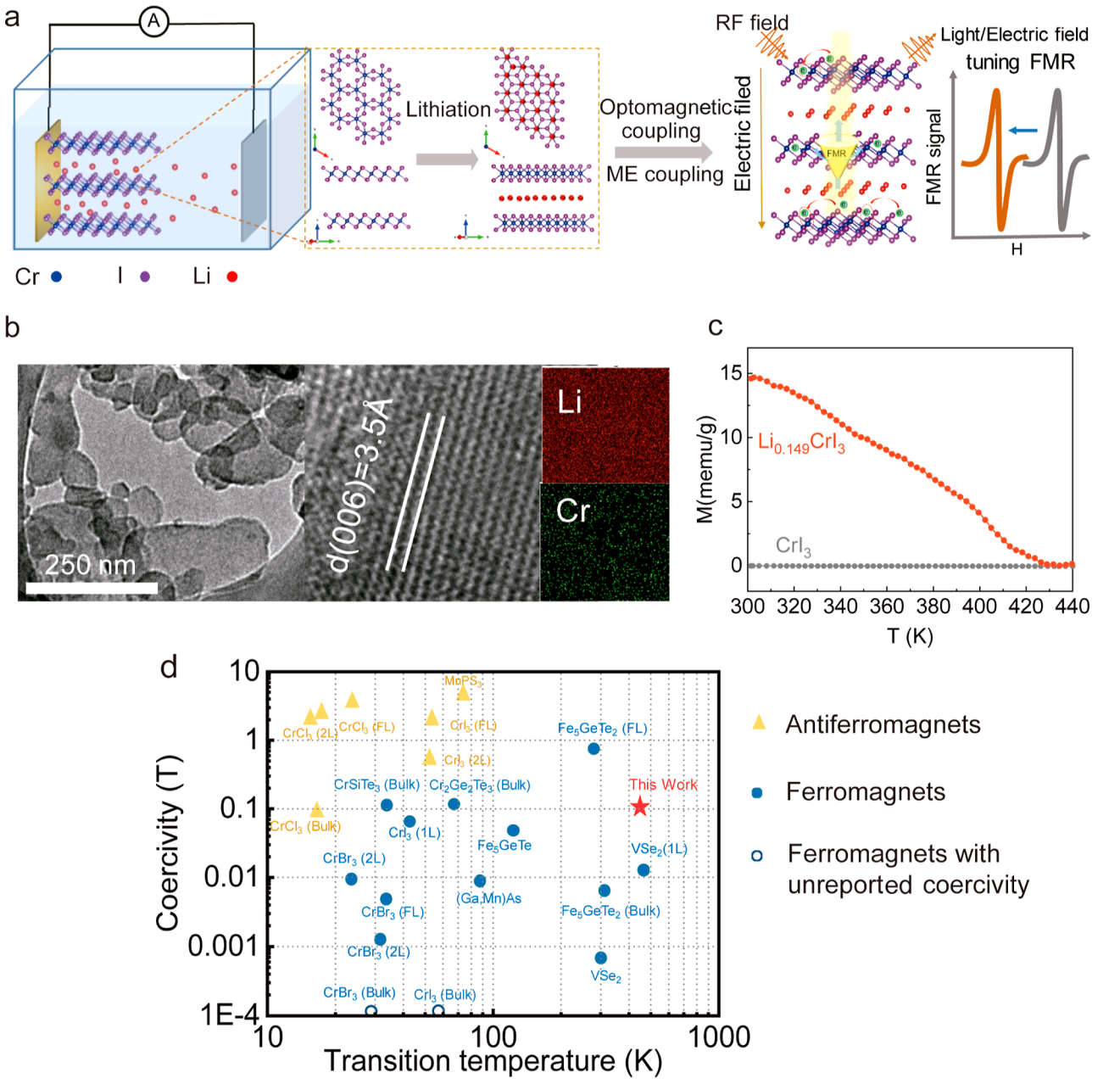

Figure 1. Characterization of electrochemically lithiated CrI_3 and its magnetic properties after lithiation. (a) Schematic of electrochemical lithiation CrI_3 shows the lithium cations penetrate into CrI_3 layers, schematic of the $Li_{0.149}CrI_3$ structure, and schematic diagram of optomagnetic and ME coupling. The green sphere represents the photoexcited electrons generated under illumination. (b) TEM image and SAED and EDS mapping of $Li_{0.149}CrI_3$. (c) Temperature-dependent magnetization of $Li_{0.149}CrI_3$. (d) Plotting of transition temperatures and coercivity of 2D magnetic materials.

the principles of electrochemistry to precisely modulate chemical interactions and packing structures, offering a versatile approach for tailoring their electronic, structural, and magnetic characteristics. Through the controlled reduction, it becomes possible to engineer the composition and atomic and electronic structures of 2D magnets, thereby influencing their band structure and magnetic exchange interactions. In this context, CrI_3 has emerged as a prominent focus in the realm of 2D vdW magnetic materials.[20] Nevertheless, its Curie temperature is approximately 45 K, whereas its bulk counterpart displays a T_C of around 51 K (Figure S1), presumably with a rhombohedral stacking structure.[21,22] The magnetic moments carried by Cr^{3+} ions are situated within a hexagonal lattice structure, coordinated by nonmagnetic I^- ions in an octahedral arrangement. Through anisotropic exchange interactions mediated by I^- ions, an ordered structure is formed within the plane. In the interlayer spacing of CrI_3, FM coupling is present, although the interactions between layers remain relatively weak. This diminished interlayer exchange interaction of CrI_3 is anticipated to be readily influenced by external perturbations, such as chemical modification, reduction, and layer intercalation, providing a distinctive avenue to alternate its magnetism.[23] Here, we report the chemical reduction of 2D CrI_3 for room temperature FM order in Li_xCrI_3. Through in situ electrochemical methods, we dynamically control the

https://doi.org/10.1021/acsnano.4c02613
ACS Nano 2024, 18, 23058−23066

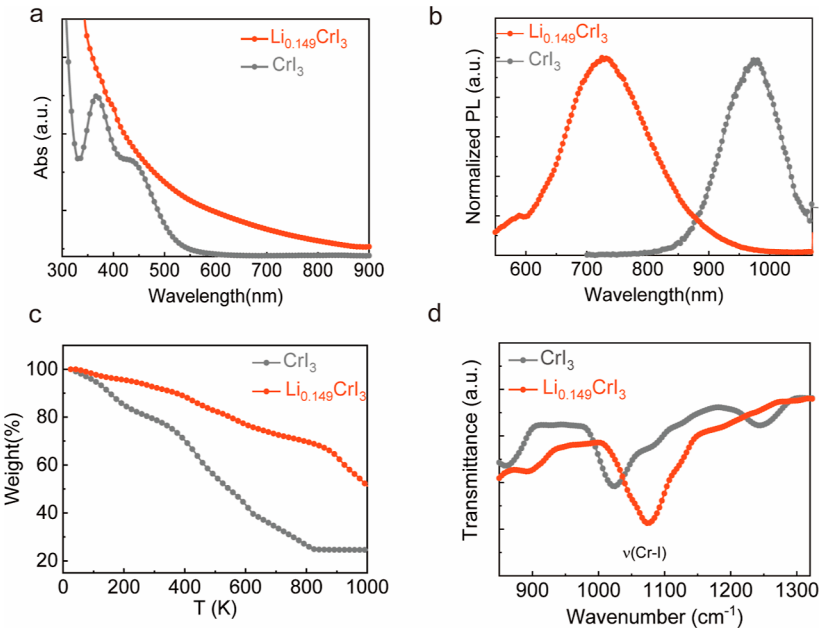

Figure 2. Spectroscopic and thermal analysis of CrI_3 and $Li_{0.149}CrI_3$. (a,b) Absorption spectra and photoluminescence (PL) spectra of CrI_3 and $Li_{0.149}CrI_3$ measured at room temperature. The excitation wavelength for the PL was a 532 nm laser. (c,d) TGA curves and FTIR spectra of CrI_3 and $Li_{0.149}CrI_3$.

lithium ion content in Li_xCrI_3, achieving effective modulation of its saturation magnetization and coercivity (H_c), and a Curie temperature of 420 K. The optimum coercivity at room temperature reaches 1120 Oe with a lithium nominal stoichiometry of 0.149. Here, lithium nominal stoichiometry (x) refers to the ratio of lithium to chromium ions. The lithiation induces tailoring of its electronic structure and optical response, leading to light-induced modulation of magnetization in Li_xCrI_3. Effective modulation of magnetism through voltage control has also been observed at room temperature. This approach not only provides a dynamic means to fine-tune magnetism but also presents an avenue for the development of electrochemically tailored magnets. More importantly, ferromagnetic resonance (FMR) tuning in 2D Li_xCrI_3 can be achieved through electric fields and noncontact optical fields. This presents a promising avenue for room-temperature, 2D MW devices.

RESULTS AND DISCUSSION

As a 2D layered material, the interlayer spacing of CrI_3 is approximately 6.6 Å.[24,25] Figure 1a presents a schematic diagram of the electrochemical process of a layered CrI_3 magnet. The large interlayer spacing, weak interlayer coupling, and 2D structure facilitate the introduction of lithium ions into the CrI_3 interlayer during the electrochemical process. Charge doping in CrI_3 effectively modulates its magnetization, coercivity, and Curie temperature,[10] and the sign of the charge carrier is crucial on whether these properties are enhanced or degraded. In this context, electrochemical lithiation involves the intercalation of lithium ions to enhance the magnetism of CrI_3. In CrI_3, Cr^{3+} ions are surrounded by six I^- ions, forming a honeycomb network (Figure 1a). Each I^- ion forms bonds with its two adjacent Cr^{3+} ions and is arranged in an edge-sharing octahedron. During the electrochemical lithiation process, the introduction of lithium ions into CrI_3 leads to a partial reduction of Cr^{3+} to Cr^{2+} (Figure 1a). The fully occupied 3d orbitals of Cr^{2+} contribute a larger magnetic moment. More importantly, the electrochemical process allows for the control of the charge and discharge processes, thereby flexibly regulating the quantity of lithium ions intercalating into the layers of CrI_3 and achieving versatile modulation of its magnetism. Moreover, FMR can be tuned effectively in $Li_{0.149}CrI_3$ through the strategic utilization of electric fields and light (Figure 1a). The noncontact modulation of FMR by light presents a compelling avenue for unlocking the potential applications of $Li_{0.149}CrI_3$ in the domain of MW devices built upon 2D materials. Figure 1b presents the transmission electron microscopy (TEM) image and selected-area electron diffraction (SAED) pattern of $Li_{0.149}CrI_3$. It is suggesting that the $Li_{0.149}CrI_3$ maintains a 2D layered structure (Figure S2). Compared to CrI_3, the diffraction peak of $Li_{0.149}CrI_3$ corresponding to the (003) crystal plane shows a significant blue shift after lithiation (Figure S2). This phenomenon may be attributed to the increase in interlayer spacing caused by the introduction of lithium ions. $Li_{0.149}CrI_3$ exhibits multilayer structures. This phenomenon may be attributed to the electrochemical delamination facilitated by the introduction of lithium ions. The d-spacing in Figure 1b represents the crystallographic phase corresponding to the (006) crystal plane of CrI_3. From the energy-dispersive system (EDS) mapping, we further confirm the chemical composition of $Li_{0.149}CrI_3$ due to the incorporation of lithium ions into CrI_3 during the lithiation process. The saturation magnetization of $Li_{0.149}CrI_3$ reaches up to 21 memu/g with a coercivity of approximately 1120 Oe. Notably, $Li_{0.149}CrI_3$ exhibits a Curie temperature of 420 K (Figure 1c). The Curie temperature of $Li_{0.149}CrI_3$ has increased by 374 K compared to that of bulk CrI_3 (51 K). The high Curie temperature of $Li_{0.149}CrI_3$ lays the foundation for studying its room temperature magnetism. As shown in Figure 1d, the lithium-intercalated CrI_3 surpasses the majority of 2D magnetic materials in terms of both Curie temperature and coercivity.

In the crystalline structure of CrI_3, the determination of the valence band maximum is predominantly influenced by the

https://doi.org/10.1021/acsnano.4c02613
ACS Nano 2024, 18, 23058−23066

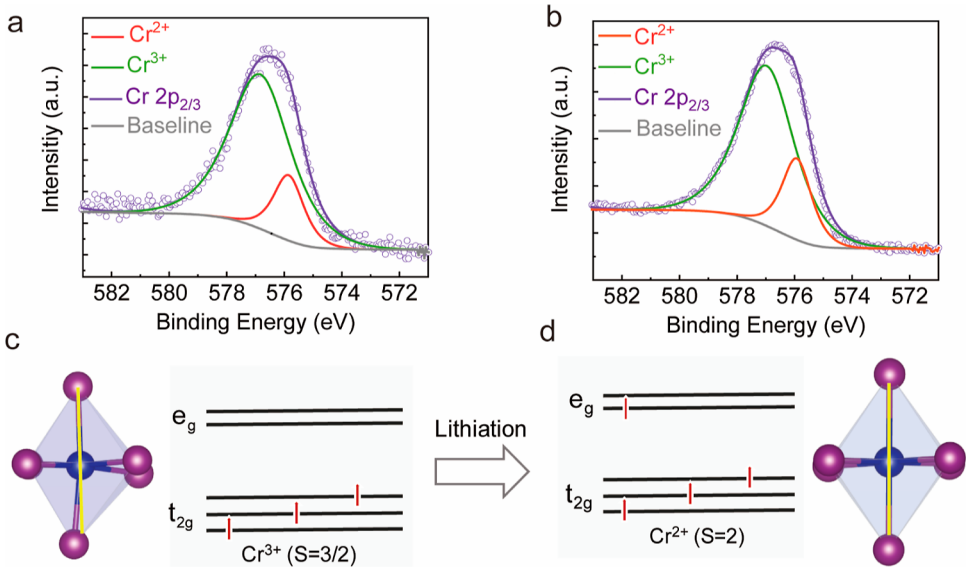

Figure 3. XPS spectra and spin configuration of Li_xCrI_3. (a) XPS spectra of $Li_{0.073}CrI_3$ with lithium nominal stoichiometry of 0.073. (b) XPS spectra of $Li_{0.149}CrI_3$ with lithium nominal stoichiometry of 0.149. (c) Spin configuration of the octahedral Cr^{3+} cation. (d) Spin configuration of Cr when the octahedral Cr^{3+} cation is reduced to coplanar Cr^{2+}.

hybridized orbitals of Cr-d and I-p, while the conduction band minimum is primarily governed by the Cr-d orbitals. Consequently, the introduction of lithium ions induces a pronounced reduction effect that significantly impacts the band structure. Figure 2a illustrates the absorption spectra of CrI_3 and $Li_{0.149}CrI_3$, in which CrI_3 exhibits obvious absorption peaks at 446 and 367 nm. However, in $Li_{0.149}CrI_3$, the absorption peaks at these two wavelengths disappeared. It only has a noticeable absorption peak around 350 nm. This indicates an obviously increase in the band gap of $Li_{0.149}CrI_3$ due to the lithium intercalation. The change in the band structure induced by lithiation inevitably affects the fluorescence spectrum of this material. As shown in Figure 2b, the fluorescence spectrum of $Li_{0.149}CrI_3$ exhibits a blue shift compared to CrI_3. This further confirms the band enlargement resulting from the lithium intercalation. The fluorescence emission peak of $Li_{0.149}CrI_3$ is at 589 nm, demonstrating a blue shift of 111 nm in comparison to that of CrI_3. This observation suggests a pronounced modification in the electronic structure of CrI_3 during the lithiation process, leading to an increased band gap. Consequently, the enhancement in photon energy released during the recombination of excited electrons leads to a blue shift in the fluorescence spectrum. As shown in Figure 2c, CrI_3 experienced a significant mass loss from thermogravimetric analysis (TGA), with a remaining weight of approximately 20%. In contrast, $Li_{0.149}CrI_3$ exhibited a substantially higher remaining weight of around 50% at the same temperature. This substantial difference in residual weight indicates the introduction of lithium ions into CrI_3. Moreover, lithiation is likely to enhance the thermal stability of $Li_{0.149}CrI_3$, reducing its decomposition rate. These may suggest the intercalation of lithium ions into CrI_3 improves the thermal stability through electrochemical lithiation. As shown in Figure 2e, the Cr−I vibrational absorption peak in CrI_3 is located at 1120 cm^{-1}, while in the Fourier transform infrared (FTIR) spectrum of $Li_{0.149}CrI_3$, the vibrational absorption peak corresponding to the Cr−I bond appears at 1160 cm^{-1} exhibiting a redshift of 40 cm^{-1}. This indicates that the introduction of lithium ions leads to a weakening of the interaction between Cr and I. New vibrational modes are additionally observed, while the frequency shift reflects the changes in the lattice structure after lithiation or alterations in atomic interactions due to the incorporation of lithium ions.

During the electrochemical lithiation process, lithium ions intercalate into the interlayers of CrI_3, providing electrons to Cr^{3+} and facilitating its reduction. To provide a further understanding of the magnetic modulation mechanism induced by lithiation, Figure 3a,b presents X-ray photoelectron spectrometry (XPS) spectra of Li_xCrI_3 with lithium nominal stoichiometry of 0.073 and 0.149, respectively. According to the XPS fitting results, Cr^{2+} is observed in the Li_xCrI_3 crystals. This suggests that a portion of Cr^{3+} in CrI_3 is reduced to Cr^{2+} by lithiation-induced reduction. Additionally, we quantitatively controlled the reduction degree of Cr^{3+} through an electrochemical method. With the lithium nominal stoichiometry increasing from 0.073 to 0.149, an analysis of the XPS fitting curves reveals that with an increase of lithiation, the content of Cr^{2+} in Li_xCrI_3 increases from 21.1 to 27.3%. This suggests that with an increased degree of lithiation, a greater proportion of Cr^{3+} is reduced to Cr^{2+}. As illustrated in Figure 3c,d of the octahedral symmetry, the d orbitals of Cr^{3+} ions undergo splitting, resulting in five orbitals, including three lower-energy triply degenerate t_{2g} orbitals (d_{xy}, d_{yz}, and d_{xz}) and two higher-energy doubly degenerate e_g orbitals (d_z^2 and $d_x^2-_y^2$). Since Cr^{3+} ions carry three electrons, these electrons occupy three t_{2g} orbitals, leading to a total spin of S = 3/2 and a coplanar framework with four I^-. Upon reduction of Cr^{3+} to Cr^{2+}, the number of electrons increases to four, as shown in Figure 3c. According to Hund's rule, three electrons occupy three t_{2g} orbitals, and the fourth electron occupies the higher-energy e_g orbital. This configuration results in an increased total spin of S = 2. Consequently, a larger magnetic moment is generated, leading to enhanced magnetization. The adjustment of such electron configurations plays a crucial role in controlling the magnetic properties of Li_xCrI_3.

An important advantage of electrochemical lithium intercalation is the ability to flexibly control the lithium ion content in the intercalated material by regulating the discharge capacity

https://doi.org/10.1021/acsnano.4c02613
ACS Nano 2024, 18, 23058−23066

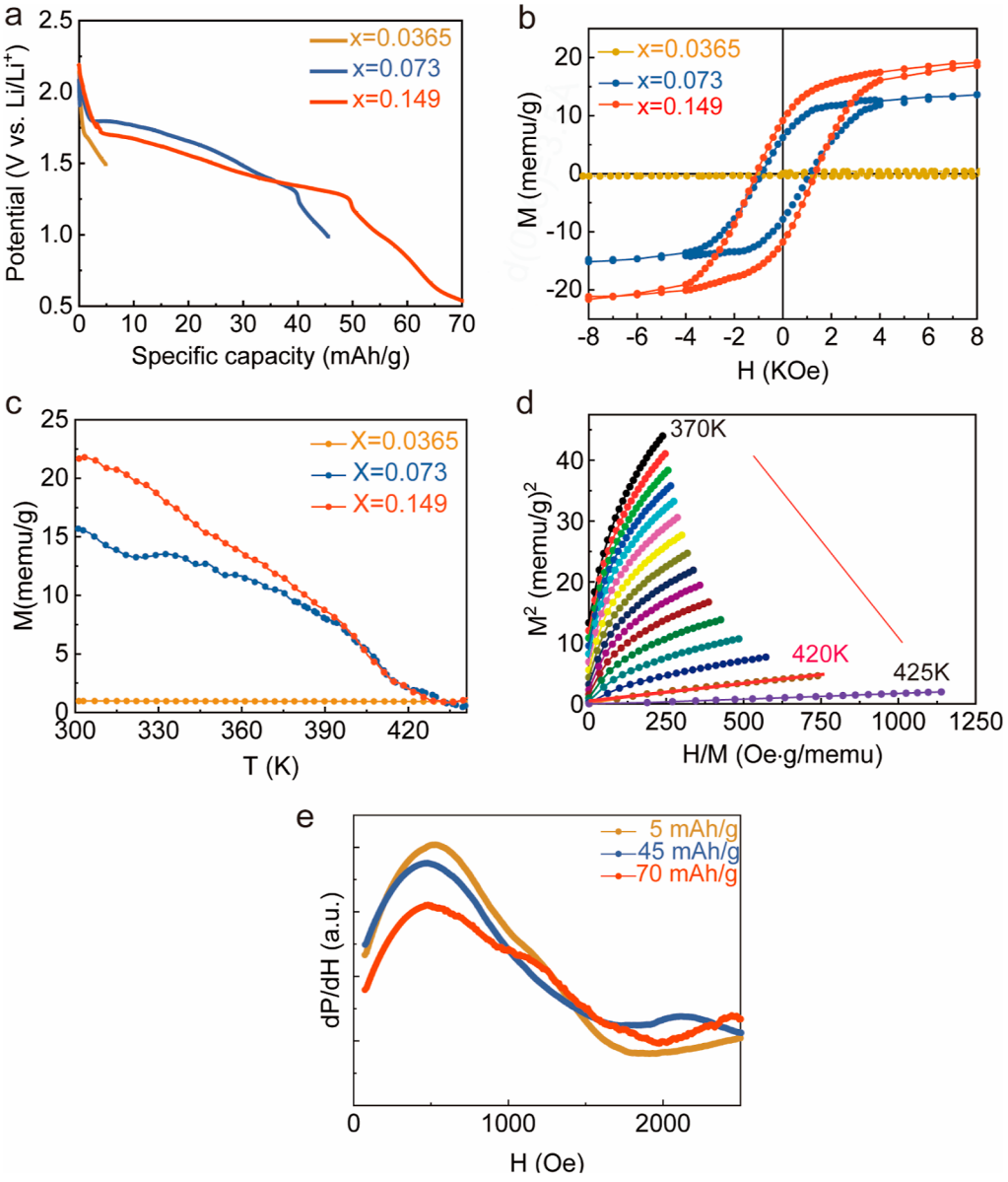

Figure 4. Lithium stoichiometric effect on magnetic properties of Li_xCrI_3. (a) Discharge curve for electrochemical lithiation. (b,c) Room temperature hysteresis loop and temperature-dependent magnetization of Li_xCrI_3 with different lithium nominal stoichiometry. (d) Arrott plots of $Li_{0.149}CrI_3$ at different temperatures around T_C. (e) Room-temperature FMR spectrum of Li_xCrI_3 that was charged at different levels from 5 to 70 mA h/g.

during the lithium intercalation process. As illustrated in Figures 4a and S4, the lithium intercalation levels corresponding to voltage values ranging from 1.5 to 0.5 V during the charging process are presented. As shown in Figure 4a, the voltage-discharge capacity curves vary with the different discharge capacities. In order to further substantiate that the room temperature magnetism in Li_xCrI_3 emanates from the reduction process involving lithium ions, we investigated the influence of lithium ion content on the magnetic properties by modulating the lithium ion concentration in Li_xCrI_3 through discharge and charge processes. In comparison to other chromium trihalides, such as $CrCl_3$ and $CrBr_3$, the FM property and higher Curie temperature of CrI_3 originate from the strong covalent interactions between chromium atoms and their nearest neighboring iodine atoms. The FM ordering in CrI_3 can be attributed to the superexchange interactions between half-filled Cr t_{2g} and empty e_g states mediated by I p orbitals. Therefore, the lithiation-induced reduction of Cr ions also alters magnetic exchange interactions, consequently affecting saturation magnetization, coercivity, and Curie temperature. As illustrated in Figure 4b,c, the saturated magnetization and H_C of Li_xCrI_3 increase with the lithium nominal stoichiometry, from 0.0365 (lithium nominal stoichiometry 5 mA h/g) to 0.149 (lithium nominal stoichiometry 70 mAh/g). The saturated magnetization and coercivity increase from 15 to 21 memu/g and from 780 to 1120 Oe, respectively. This is attributed to the reduction of Cr^{3+} to Cr^{2+}, which not only increases the magnetic moment but also enhances magnetic exchange interactions. This leads to an increase in the saturation magnetization, coercivity, and Curie temperature, as previously demonstrated. We further determined the Curie temperature of $Li_{0.149}CrI_3$ using standard Arrott plots. When the curve nearly extrapolates to the origin

https://doi.org/10.1021/acsnano.4c02613
ACS Nano 2024, 18, 23058−23066

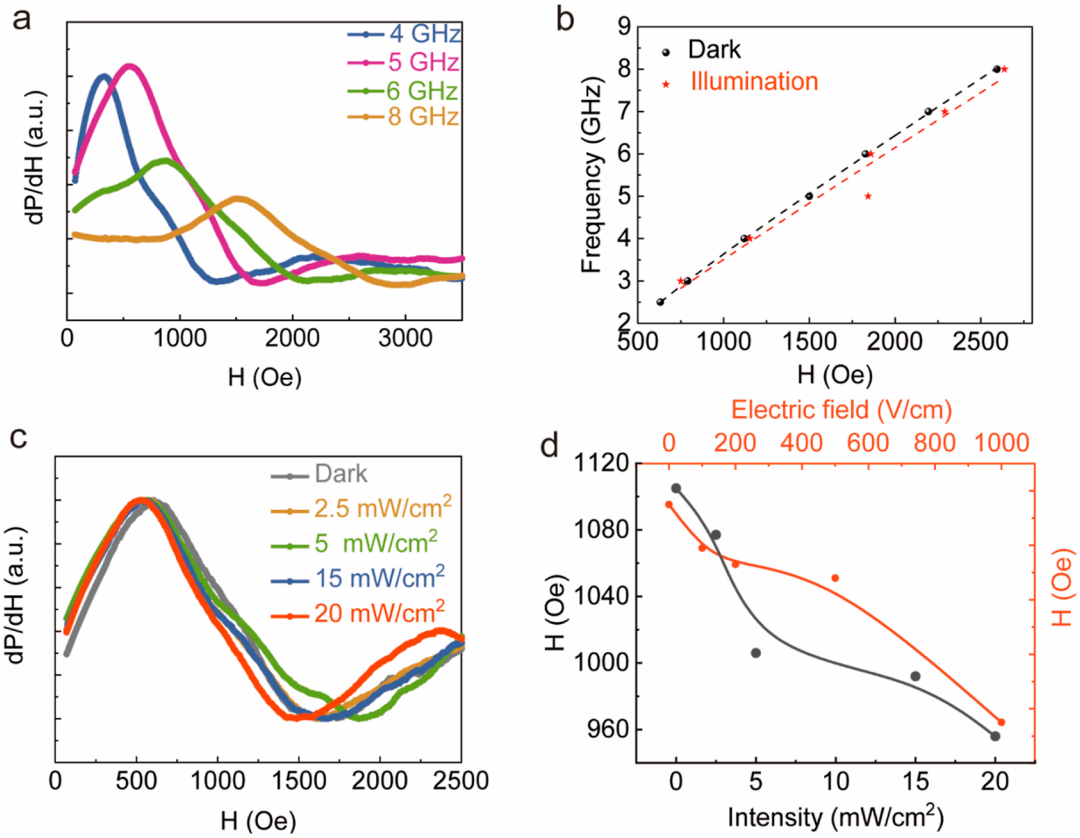

Figure 5. Optomagnetic and ME coupling of $Li_{0.149}CrI_3$. (a) Room-temperature FMR spectra at different RF conditions. (b) Room-temperature FMR spectra of $Li_{0.149}CrI_3$ at the resonance frequency as a function of resonance field. (c) Illumination intensity dependent FMR spectra and resonance field under 4 GHz for $Li_{0.149}CrI_3$, which were measured at room temperature. The excitation wavelength of the light was a 532 nm laser. (d) Electric field and illumination intensity-dependent resonance field under 4 GHz for $Li_{0.149}CrI_3$. The excitation wavelength of the light was a 532 nm laser.

(0, 0) at 420 K, it indicates that the Curie temperature is approximately 420 K.

In order to further confirm the enhancement of the Curie temperature of CrI_3 through lithium-ion reduction, we prepared Li_xCrI_3 samples by using the solvation lithiation method. It was observed that Li_xCrI_3 treated with solvation lithiation exhibited magnetic properties at room temperature (Figure S5). Both the saturation magnetization and coercivity increased with the lithium ion concentration in the lithiation solution. Additionally, Li_xCrI_3 exhibits room-temperature magnetic anisotropy after solvation lithiation (Figure S6). This indicates that solvation lithiation also achieves room-temperature magnetic ordering by introducing lithium ions. In Figure 4d, the FMR of Li_xCrI_3 after charging is presented. We charged the Li_xCrI_3 and observed their FMR signals at different delithiation levels, corresponding to 5, 45, and 70 mA h/g, respectively. As lithium nominal stoichiometry increases from 5 to 70 mA h/g, the FMR signal gradually weakens. This is attributed to the charge process leading to delithiation from the interlayer structure. Consequently, this results in Cr^{2+} originally formed due to lithium ion reduction back to Cr^{3+}, thereby diminishing magnetic interactions and magnetic moments.

The enhancement of magnetism via gate voltage in metal-oxide-semiconductor field-effect transistor devices has been notable, yet it comes with inherent limitations.[26,27] First, the material's phase transition typically necessitates a high gate voltage to produce enough induced carriers for magnetism enhancement. However, this high voltage can potentially cause the breakdown of the dielectric layer. Second, the electric field effect produced by the gate voltage is usually limited to a shallow surface layer. In contrast, electrochemical methods can achieve magnetic manipulation at low voltage conditions at room temperature, where the ions in the electrolyte ionic liquid migrate under the voltages.[28] Under the influence of an electric field, these ions can either intercalate into or migrate into or out of the magnetic material, thereby controlling its magnetism via redox reactions. Consequently, electrochemical control can be conducted at relatively low voltages, enabling low-voltage operation with greater depth of control compared to electrostatic gating.[27] Additionally, by controlling the amount of ion intercalation, in situ quantitative control of magnetism can be achieved.[19] The low spatial hindrance in 2D structures further enhances the migration rate of lithium ions and other alkali metal ions. However, it should be noted that electrochemical methods may introduce a certain contamination.

Apart from electrochemical modulation of the FM property, optomagnetic and magnetoelectric (ME) coupling effects also are observed in $Li_{0.149}CrI_3$. As shown in Figures 5a and S7, $Li_{0.149}CrI_3$ exhibits a pronounced FMR signal at room temperature, further confirming its magnetic order. As the frequency continues to increase, the response magnetic field consistently shifts to the right. Owing to the intrinsic nature of the gyromagnetic ratio in magnetic materials, the response magnetic field intensity exhibits a direct proportionality to the

https://doi.org/10.1021/acsnano.4c02613
ACS Nano 2024, 18, 23058−23066

resonance frequency for spin resonance absorption. Consequently, with an increase in frequency, there is a corresponding augmentation in the response magnetic field. We conducted room-temperature FMR of $Li_{0.149}CrI_3$ under illuminated and dark conditions. By comparing the fitting curves of the magnetic field under dark and illuminated conditions at 20 mW/cm^2, we observed that the slope of the curve under light illumination was noticeably smaller than that under dark conditions (Figures 5b and S8). The magnetization of $Li_{0.149}CrI_3$ increased by approximately 18.4% under light excitation. In order to further investigate light-modulated magnetism, we conducted tests on the FMR spectra under varying light intensities. When the incident light intensity reaches 20 mw/cm^2, as illustrated in Figure 5c,d, the resonance field of $Li_{0.149}CrI_3$ decreased from 1148 to 963 Oe. This further confirms an increase in the magnetization of $Li_{0.149}CrI_3$ under light illumination. In chromium-halide-based FM semiconductors, the origin of strong magneto-optical coupling lies in the reduction process induced by optical excitation, converting Cr^{3+} to Cr^{2+}. Within CrI_3, photoinduced electronic transitions result in the capture of free electrons generated by optical excitation by Cr^{3+}, leading to the formation of Cr^{2+} centers and triggering a reduction effect.[29−31] Hence, optical excitation induces the generation of photogenerated charges and a reduction effect in $Li_{0.149}CrI_3$, thereby inducing the capture of an increased number of excited electrons from the conduction band by Cr^{3+} (Figure S9). Consequently, this phenomenon precipitates a heightened optical magnetic response.[32] This optically induced electron transfer process plays a crucial role in shaping the material properties, providing a key mechanism for the enhancement of magnetism. This light-induced modulation of FMR in 2D $Li_{0.149}CrI_3$ furthers the study and application of noncontact 2D nanoscale MW devices. In addition, an electric-field-induced magnetization modulation was observed in $Li_{0.149}CrI_3$, as depicted in Figures 5d and S10. With the electric field increasing from 100 to 1000 V/cm, the response field of $Li_{0.149}CrI_3$ is decreased from 1179 to 1115 Oe. This indicates an increase in magnetization under an electric field. This may arise from the capture of injected electrons by Cr^{3+}, leading to the formation of Cr^{2+} centers and triggering a reduction effect. Therefore, under the electric field injection of electrons, the magnetization intensity is enhanced due to the reduction of Cr^{3+}, while the response field decreases with the increasing electric field intensity. The combined modulation of light and electric fields enables the use of $Li_{0.149}CrI_3$ for magnetoelectronic devices and its development in the realm of magnetic materials.

CONCLUSIONS

In conclusion, we successfully prepared a room-temperature 2D magnet by electrochemically lithiating CrI_3, thereby reducing Cr^{3+} to Cr^{2+}. The enhanced magnetic exchange interactions resulting from lithiation increase the Curie temperature of Li_xCrI_3 from 45 to 420 K. Importantly, we demonstrated precise control over the lithium ion content between the layers of the 2D structure through charge and discharge processes, allowing for flexible modulation of the magnetic properties. Furthermore, a significant aspect of our findings is the ability to achieve noncontact control of FMR through optical excitation. This makes it possible for future applications of 2D noncontact MW devices. The outcomes of this research not only represent a significant advancement in the development of magnetic materials but also allow for the design and utilization of tunable 2D MW devices.

EXPERIMENTAL SECTION

Electrochemical Lithiation of CrI_3. The cathode consisted of a copper foil covered with a CrI_3 powder (Ossila, ≥ 99.995%) mixture on one side. The mixture, comprising CrI_3, conductive carbon black (MSE Supplies), and polyvinylidene fluoride in a weight ratio of 40%:20%:20% was dissolved in 1-methyl-2-pyrrolidone solvent and stirred for 12 h. The resulting fluid was evenly applied to the copper foil and heated at 50 °C on a hot plate for 12 h. The cathode, with the CrI_3 mixture-covered copper foil and a lithium piece serving as the anode were secured by copper clips and immersed in a 1 mol/L electrolyte prepared by dissolving lithium perchloride in anhydrous propylene carbonate (Sigma-Aldrich, 99.7%). Voltammetry was conducted using a Keithley 2450 instrument. During the discharging process, a negative 0.1 mA current was applied, and the cathode voltage was monitored over time. Specific discharge periods concluded at different voltages for varying lithiation levels. Subsequently, the electrochemically lithiated sample was collected and dried for measurements, with all procedures carried out in a N_2 glovebox.

Solvation Lithiation of CrI_3. A mixture of 231.3 mg of 1,2-dihydroacenaphthylene and 52, 104, and 171 mg of lithium in 8 mL of tetrahydrofuran (THF) solvent was stirred for 3 h. The filtered solution was introduced into a 20 mL glass vessel with a 5 mL THF solution, alongside 52 mg of the CrI_3 powder. After a week of stirring, the product underwent washing with 15 mL of THF solvent two or three times and subsequent vacuum-drying. All procedures were carried out in an N_2 glovebox.

The investigation of magnetic properties and light/electric field tuning FMR was conducted through the utilization of a MicroSense EZ7−380 V vibrating sample magnetometer and FMR. The assessment included FMR experiments that incorporated MW irradiation, implemented via a continuous wave (CW) FMR system. This particular system featured a CW broadband MW source (Agilent N5172B-520; 1−19 GHz) connected to a coplanar waveguide, with the sample strategically positioned in immediate proximity. Furthermore, a power-adjustable 405 nm laser served as the excitation light source.

Thermal analysis, UV−vis absorption measurements, and PL were carried out using specialized instruments. Thermal transitions were characterized utilizing a PerkinElmer differential scanning calorimetry 7 differential scanning calorimeter, located in Shelton, CT, with experiments executed at a heating rate of 5 °C min^{-1}. The evaluation of thermal degradation was conducted by employing a thermogravimetric analyzer (TGA) (SDT Q600, TA Instruments., USA) under a nitrogen (N_2) atmosphere. UV−vis absorption spectra were obtained using an Agilent Cary 7000 UV−vis-near-IR spectrophotometer. For room-temperature PL measurements, the samples were mounted in a dewar and kept in a vacuum during the measurements. A home-built confocal microscope system was used to focus the laser onto the samples with a ∼2 μm beam spot. The PL signals were collected through a spectrometer (Princeton Instrument) equipped with a silicon charge-coupled device (Andor). The PL measurements were performed with a continuous wave (CW) laser centered at 532 nm.

https://doi.org/10.1021/acsnano.4c02613
ACS Nano 2024, 18, 23058−23066

ASSOCIATED CONTENT

Supporting Information

The Supporting Information is available free of charge at https://pubs.acs.org/doi/10.1021/acsnano.4c02613.

Hysteresis loop and temperature-dependent magnetization curve of CrI_3; TEM, Hysteresis loop and temperature-dependent magnetization curve of Li_xCrI_3; hysteresis loops and magnetic anisotropy of Li_xCrI_3 prepared by solution lithiation; light intensity, electric field, and frequency-dependent FMR of Li_xCrI_3; and dielectric variation curves of Li_xCrI_3 under different light intensities (PDF)

AUTHOR INFORMATION

Corresponding Author

Shenqiang Ren − *Department of Materials Science and Engineering, University of Maryland, College Park, Maryland 20742, United States;* orcid.org/0000-0002-9987-3316; Email: sren@umd.edu

Authors

Zhongxuan Wang − *Department of Materials Science and Engineering, University of Maryland, College Park, Maryland 20742, United States;* orcid.org/0000-0003-1664-4639

Huafei Zheng − *Department of Chemistry and Biochemistry, University of Maryland, College Park, Maryland 20742, United States;* orcid.org/0000-0001-6412-8212

Amy Chen − *Department of Materials Science and Engineering, University of Maryland, College Park, Maryland 20742, United States*

Lei Ma − *Department of Chemical and Biological Engineering, Rensselaer Polytechnic Institute, Troy, New York 12180, United States*

Stephanie J. Hong − *Department of Chemistry and Biochemistry, University of Maryland, College Park, Maryland 20742, United States;* orcid.org/0000-0002-1878-0338

Efrain E. Rodriguez − *Department of Chemistry and Biochemistry, University of Maryland, College Park, Maryland 20742, United States;* orcid.org/0000-0001-6044-1543

Taylor J. Woehl − *Department of Chemical and Biomolecular Engineering, University of Maryland, College Park, Maryland 20742, United States;* orcid.org/0000-0002-4000-8280

Su-Fei Shi − *Department of Chemical and Biological Engineering, Rensselaer Polytechnic Institute, Troy, New York 12180, United States; Department of Physics, Carnegie Mellon University, Pittsburgh, Pennsylvania 15213, United States*

Thomas Parker − *Army Research Laboratory, Aberdeen Proving Ground, Aberdeen, Maryland 21005, United States*

Complete contact information is available at: https://pubs.acs.org/10.1021/acsnano.4c02613

Author Contributions

S.R. and Z.W. conceived the idea. Z.W. designed the study and conducted all sample syntheses and processing, UV−vis absorption measurements, and Raman and Fourier transform spectroscopies. H.Z. did the hysteresis loops of Li_xCrI_3 and CrI_3. S.J.H. performed the TGA. L.M. and S.-F.S. performed photoluminescence spectra of Li_xCrI_3 and CrI_3. A.C. and T.J.W. contributed to TEM images and SAED patterns. T.P. performed the XPS data analysis. Z.W. wrote the manuscript with comments and inputs from all authors. All authors have given approval to the final version of the manuscript.

Notes

The authors declare no competing financial interest.

ACKNOWLEDGMENTS

The U.S. Department of Energy, Office of Basic Energy Sciences, Division of Materials Sciences and Engineering supports S.R. under Award DE-SC0024796. S.-F.S. acknowledges the support from NSF (Career Grant DMR-1945420, DMR-2104902, and ECCS-2139692). E.E.R. and H.Z. thank the National Science Foundation, NSF DMR-2113682, for financial assistance.

REFERENCES

(1) Nozaki, T.; Shiota, Y.; Miwa, S.; Murakami, S.; Bonell, F.; Ishibashi, S.; Kubota, H.; Yakushiji, K.; Saruya, T.; Fukushima, A.; et al. Electric-Field-Induced Ferromagnetic Resonance Excitation in an Ultrathin Ferromagnetic Metal Layer. *Nat. Phys.* **2012**, *8* (6), 491−496.

(2) Owens, J. M.; Collins, J. H.; Carter, R. L. System Applications of Magnetostatic Wave Devices. *Circuits Syst. Signal Process.* **1985**, *4* (1−2), 317−334.

(3) Cherepanov, V.; Kolokolov, I.; L'Vov, V. The Saga of YIG: Spectra, Thermodynamics, Interaction and Relaxation of Magnons in a Complex Magnet. *Phys. Rep.* **1993**, *229* (3), 81−144.

(4) Cai, Z.; Su, L.; Wang, H.; Niu, M.; Tao, L.; Lu, D.; Xu, L.; Li, M.; Gao, H. Alternating Multilayered Si_3N_4/SiC Aerogels for Broadband and High-Temperature Electromagnetic Wave Absorption up to 1000 °C. *ACS Appl. Mater. Interfaces* **2021**, *13* (14), 16704−16712.

(5) Balashov, T.; Buczek, P.; Sandratskii, L.; Ernst, A.; Wulfhekel, W. Magnon Dispersion in Thin Magnetic Films. *J. Phys.: Condens. Matter* **2014**, *26* (39), 394007.

(6) Shiota, Y.; Nozaki, T.; Bonell, F.; Murakami, S.; Shinjo, T.; Suzuki, Y. Induction of Coherent Magnetization Switching in a Few Atomic Layers of FeCo Using Voltage Pulses. *Nat. Mater.* **2012**, *11* (1), 39−43.

(7) Matsukura, F.; Tokura, Y.; Ohno, H. Control of Magnetism by Electric Fields. *Nat. Nanotechnol.* **2015**, *10* (3), 209−220.

(8) Wang, W.-G.; Li, M.; Hageman, S.; Chien, C. L. Electric-Field-Assisted Switching in Magnetic Tunnel junctions. *Nat. Mater.* **2012**, *11* (1), 64−68.

(9) Cai, K.; Yang, M.; Ju, H.; Wang, S.; Ji, Y.; Li, B.; Edmonds, K. W.; Sheng, Y.; Zhang, B.; Zhang, N.; Liu, S.; Zheng, H.; Wang, K. Electric Field Control of Deterministic Current-Induced Magnetization Switching in a Hybrid Ferromagnetic/Ferroelectric Structure. *Nat. Mater.* **2017**, *16* (7), 712−716.

(10) Jiang, S.; Li, L.; Wang, Z.; Mak, K. F.; Shan, J. Controlling Magnetism in 2d CrI_3 by Electrostatic Doping. *Nat. Nanotechnol.* **2018**, *13* (7), 549−553.

(11) Gong, C.; Zhang, X. Two-Dimensional Magnetic Crystals and Emergent Heterostructure Devices. *Science* **2019**, *363* (6428), No. eaav4450.

(12) Jiang, S.; Shan, J.; Mak, K. F. Electric-Field Switching of Two-Dimensional Van Der Waals Magnets. *Nat. Mater.* **2018**, *17* (5), 406−410.

(13) Gibertini, M.; Koperski, M.; Morpurgo, A. F.; Novoselov, K. S. Magnetic 2d Materials and Heterostructures. *Nat. Nanotechnol.* **2019**, *14* (5), 408−419.

(14) Zhang, Y.; Chu, J.; Yin, L.; Shifa, T. A.; Cheng, Z.; Cheng, R.; Wang, F.; Wen, Y.; Zhan, X.; Wang, Z.; He, J. Ultrathin Magnetic 2D Single-Crystal CrSe. *Adv. Mater.* **2019**, *31* (19), 1900056.

(15) Gong, C.; Li, L.; Li, Z.; Ji, H.; Stern, A.; Xia, Y.; Cao, T.; Bao, W.; Wang, C.; Wang, Y.; Qiu, Z. Q.; Cava, R. J.; Louie, S. G.; Xia, J.;

Zhang, X. Discovery of Intrinsic Ferromagnetism in Two-Dimensional Van Der Waals Crystals. *Nature* **2017**, *546* (7657), 265−269.
(16) Liang, S.; Xie, T.; Blumenschein, N. A.; Zhou, T.; Ersevim, T.; Song, Z.; Liang, J.; Susner, M. A.; Conner, B. S.; Gong, S.-J.; Wang, J.-P.; Ouyang, M.; Žutić, I.; Friedman, A. L.; Zhang, X.; Gong, C. Small-Voltage Multiferroic Control of Two-Dimensional Magnetic Insulators. *Nat. Electron.* **2023**, *6* (3), 199−205.
(17) Li, T.; Jiang, S.; Sivadas, N.; Wang, Z.; Xu, Y.; Weber, D.; Goldberger, J. E.; Watanabe, K.; Taniguchi, T.; Fennie, C. J.; Fai Mak, K.; Shan, J. Pressure-Controlled Interlayer Magnetism in Atomically Thin CrI_3. *Nat. Mater.* **2019**, *18* (12), 1303−1308.
(18) Perlepe, P.; Oyarzabal, I.; Mailman, A.; Yquel, M.; Platunov, M.; Dovgaliuk, I.; Rouzières, M.; Négrier, P.; Mondieig, D.; Suturina, E. A.; Dourges, M.-A.; Bonhommeau, S.; Musgrave, R. A.; Pedersen, K. S.; Chernyshov, D.; Wilhelm, F.; Rogalev, A.; Mathonière, C.; Clérac, R. Metal-organic magnets with large coercivity and ordering temperatures up to 242°C. *Science* **2020**, *370* (6516), 587−592.
(19) Huang, Y.; Zhang, Q.; Li, Y. C.; Yao, Y.; Hu, Y.; Ren, S. Chemical Tuning Meets 2d Molecular Magnets. *Adv. Mater.* **2023**, *35* (5), 2208919.
(20) Huang, B.; Clark, G.; Navarro-Moratalla, E.; Klein, D. R.; Cheng, R.; Seyler, K. L.; Zhong, D.; Schmidgall, E.; McGuire, M. A.; Cobden, D. H.; Yao, W.; Xiao, D.; Jarillo-Herrero, P.; Xu, X. Layer-Dependent Ferromagnetism in a Van Der Waals Crystal Down to the Monolayer Limit. *Nature* **2017**, *546* (7657), 270−273.
(21) Wahab, D. A.; Augustin, M.; Valero, S. M.; Kuang, W.; Jenkins, S.; Coronado, E.; Grigorieva, I. V.; Vera-Marun, I. J.; Navarro-Moratalla, E.; Evans, R. F. L.; et al. Quantum Rescaling, Domain Metastability, and Hybrid Domain-Walls in 2d CrI_3 Magnets. *Adv. Mater.* **2021**, *33* (5), 2004138.
(22) Song, T.; Fei, Z.; Yankowitz, M.; Lin, Z.; Jiang, Q.; Hwangbo, K.; Zhang, Q.; Sun, B.; Taniguchi, T.; Watanabe, K.; McGuire, M. A.; Graf, D.; Cao, T.; Chu, J.-H.; Cobden, D. H.; Dean, C. R.; Xiao, D.; Xu, X. Switching 2d Magnetic States Via Pressure Tuning of Layer Stacking. *Nat. Mater.* **2019**, *18* (12), 1298−1302.
(23) Wang, B.; Wu, Q.; Zhang, Y.; Guo, Y.; Zhang, X.; Zhou, Q.; Dong, S.; Wang, J. High Curie-Temperature Intrinsic Ferromagnetism and Hole Doping-Induced Half-Metallicity in Two-Dimensional Scandium Chlorine Monolayers. *Nanoscale Horiz.* **2018**, *3* (5), 551−555.
(24) McGuire, M. A.; Dixit, H.; Cooper, V. R.; Sales, B. C. Coupling of Crystal Structure and Magnetism in the Layered, Ferromagnetic Insulator CrI_3. *Chem. Mater.* **2015**, *27* (2), 612−620.
(25) Zhang, Y.; Liu, J.; Deng, R.; Shi, X.; Tang, H.; Chen, H.; Yuan, H. Electronic Structure, Magnetoresistance and Spin Filtering in Graphene|2 Monolayer-CrI_3|Graphene Van Der Waals Magnetic Tunnel Junctions. *RSC Adv.* **2022**, *12* (44), 28533−28544.
(26) Ahn, C. H.; Triscone, J.-M.; Mannhart, J. Electric Field Effect in Correlated Oxide Systems. *Nature* **2003**, *424* (6952), 1015−1018.
(27) Ahn, C.; Bhattacharya, A.; Di Ventra, M.; Eckstein, J. N.; Frisbie, C. D.; Gershenson, M. E.; Goldman, A. M.; Inoue, I. H.; Mannhart, J.; Millis, A. J.; et al. Electrostatic Modification of Novel Materials. *Rev. Mod. Phys.* **2006**, *78* (4), 1185−1212.
(28) Deng, Y.; Yu, Y.; Song, Y.; Zhang, J.; Wang, N. Z.; Sun, Z.; Yi, Y.; Wu, Y. Z.; Wu, S.; Zhu, J.; et al. Gate-Tunable Room-Temperature Ferromagnetism in Two-Dimensional Fe_3GeTe_2. *Nature* **2018**, *563* (7729), 94−99.
(29) Mosiniewicz-Szablewska, E.; Szymczak, H. Photomagnetic Effect in the $CdCr_2Se_4$ Ferromagnetic Semiconductor. *Phys. Rev. B* **1993**, *47* (14), 8700−8705.
(30) Mosiniewicz-Szablewska, E.; Szymczak, H. Photoinduced Changes in the Ferromagnetic Resonance of $CdCr_2Se_4$ Single Crystals. *J. Magn. Magn. Mater.* **1992**, *104*−*107*, 986−988.
(31) Lems, W.; Rijnierse, P.; Bongers, P.; Enz, U. Photomagnetic Effect in a Chalcogenide Spinel. *Phys. Rev. Lett.* **1968**, *21* (24), 1643−1645.
(32) Singamaneni, S. R.; Martinez, L. M.; Niklas, J.; Poluektov, O. G.; Yadav, R.; Pizzochero, M.; Yazyev, O. V.; McGuire, M. A. Light Induced Electron Spin Resonance Properties of Van Der Waals CrX_3 (X = Cl, I) Crystals. *Appl. Phys. Lett.* **2020**, *117* (8), 082406.

https://doi.org/10.1021/acsnano.4c02613
ACS Nano 2024, 18, 23058−23066